Journal of Catalysis 279 (2011) 155–162

Contents lists available at ScienceDirect

Journal of Catalysis

journal homepage: www.elsevier.com/locate/jcat

Orientated intercalation of tartrate as chiral ligand to impact asymmetric catalysis

Huimin Shi, Jing He *

State Key Laboratory of Chemical Resource Engineering, Beijing University of Chemical Technology, Beijing 100029, PR China

ARTICLE INFO

Article history:
Received 15 November 2010
Revised 11 January 2011
Accepted 13 January 2011
Available online 12 February 2011

Keywords:
Layered double hydroxide
Tartrate ligand
Interlayer orientation
Ti (IV) coordination
Asymmetric sulfoxidation

ABSTRACT

Pre-immobilization of chiral ligands to coordinate with metal centers is one common strategy for the heterogenization of asymmetric metal–complex catalysts. But how the pre-immobilization of chiral ligands made impact on their coordination to metal centers and subsequently asymmetric catalysis has seldom been investigated. Here, in this work, L-tartrate anions as chiral ligands are first intercalated into the interlayer space of Mg/Al layered double hydroxide (LDH) and then in situ coordinated to the Ti (IV) centers. The tartrates are controlled in either perpendicular-standing or flat-lying arrangement in the interlayer region by altering the solvent for intercalation reaction. The perpendicular-standing interlayer tartrates are found to bear both C—O—Ti and C=O—Ti coordination modes, while the flat-lying interlayer tartrates hold only the C—O—Ti coordination mode. The complex with the Ti (IV) center coordinated to perpendicular-standing interlayer tartrate in both C—O—Ti and C=O—Ti modes not only displays higher catalytic activity in the asymmetric sulfoxidation but also produces higher enantioselectivity for sulfoxide.

1. Introduction

In more recent years, the heterogenization of homogeneous chiral catalysts has been a great concern in the field of asymmetric catalysis [1]. In the preparation of heterogeneous metal–complex catalysts, the pre-immobilization of chiral ligands to coordinate with metal centers is one common strategy. A variety of chiral metal–complexes were heterogenized in this way. For example, the BINAP (2,2′-bis(diphenylphosphanyl)-1,1′-binapthyl) skeleton was incorporated into a polyester chain to coordinate with Ru (II) centers [2]. Imidazoindole phosphine was immobilized on amphiphilic resin to coordinate with Pd (II) centers [3]. Tartarte ligands were immobilized on polymers [4,5], amorphous silica, and mesoporous material [6] to coordinate with Ti (IV) centers. Pyridine-bis(oxazoline) was grafted on polymers [7] and mesoporous silica [8], electrostatically adsorbed on Laponite and Nafion/silica nanocomposites [9], to coordinate with Ru (II) or Cu (II). Ferrocene [10] and amino alcohol [11] were grafted in the pores of mesoporous silicas to coordinate with Pd (II) or Cu (II). The relationship between the accessibility of active sites and activities [2,7,8], and the steric effects of supports on enantioselectivity [2,6,11] have generally been concerned. But no report discussed the coordination of pre-immobilized chiral ligands to metal centers and its consequent effects on the asymmetric catalysis.

Layered double hydroxides (LDHs), the so-called anionic clays, consisting of positively charged brucite-like layers and interlayer exchangeable anions [12], provide a bi-dimensional interlayer region to anisotropically accommodate the guest anions at nanoscale [13]. The positive brucite-like layers of LDHs are capable of electrostatically inducing the intercalated guest anions to take orientation or be arranged in order [14], by which influencing the physicochemical properties of the resulting intercalates [15–17]. In the case of poly (diacetylenecarboxylates) incorporated LDHs, for example, the possible different orientations of interlayer guests were proposed to be responsible for the observed reversible thermal color changes [15]. Additionally, the orientation of interlayer anions was found to influence the diffusion of ingoing species, thus making impact on the accessibility of active sites in catalytic reactions [16] or the exchangeability of interlayer anions in ion-exchange reactions [17]. The optimum accessibility of the metal centers was provided by a perpendicular orientation of [Co(II)-tetrasulfophthalocyanine]$^{4-}$ in the interlayer gallery of LDHs [16]. A maximum adsorption amount of 2,4-dichlorophenoxyacetic was observed on the LDHs with the interlayer nitrate arranged perpendicularly to the brucite-like layers [17]. The organic anions intercalated in LDHs were employed as chelating ligands to metal cations [18–21]. The catalysis of the in situ coordinated metal sites was investigated [21]. Chiral organic guests, such as S-BINOL [22], were also introduced into the interlayer region of LDHs as chiral auxiliaries. The intercalated auxiliaries were supposed to serve as asymmetric-inducing reagents. Unfortunately, almost no enantiomer excess was observed, although high catalytic activities were achieved.

In our previous work [23,24], the heterogeneous titanium–tartrate catalysts were prepared by intercalating LDH hosts with

* Corresponding author. Fax: +86 10 64425385.
E-mail address: jinghe@263.net.cn (J. He).

0021-9517/$ - see front matter © 2011 Published by Elsevier Inc.
doi:10.1016/j.jcat.2011.01.012

pre-formed Ti (IV)–tartrate complex. The arrangement of interlayer titanium–tartrate and thus arrangement-dependent interlayer spacing were controlled by tuning the charge density of the brucite-like layers [23]. The effects of interlayer anion arrangement and interlayer spacing on the asymmetric sulfoxidation were discussed [24]. In this paper, the heterogenization of chiral Ti (IV) complex has been implemented by pre-immobilizing chiral tartrate ligands in the interlayer region of LDHs. The interlayer tartrate ligands have been controlled in different arrangements. The dependence of tartrate–Ti (IV) coordination modes and consequently asymmetric catalytic sulfoxidation on the orientation of tartrate has been discussed.

2. Experimental

2.1. Materials

L-tartaric acid (Aldrich, 99.5%), sodium L-(+)-tartrate dehydrate (Alfa Aesar, 99.0–101.0%), $Ti(OPr^i)_4$ (Aldrich, 97%), methyl phenyl sulfide (MPS, Acros, 99%), methyl phenyl sulfoxide (MPSO, Aldrich, 97%), and H_2O_2 (30% aqueous solution) were used as received without further purification. $Mg(NO_3)_2{\cdot}6H_2O$, $NO_3)_3{\cdot}9H_2O$, NaOH, anhydrous Na_2CO_3, *n*-butanol, CH_2Cl_2, CH_3OH, and CH_3CN are all of analytical purity. In prior to use, CH_2Cl_2 was first treated in 4 Å zeolite overnight, and then distilled in CaH_2 to remove the water.

2.2. Preparation

The LDH with carbonate as interlayer anion was synthesized with separate nucleation and aging steps. Typically, a solution of 0.18 mol of $Mg(NO_3)_2{\cdot}6H_2O$ and 0.072 mol of $Al(NO_3)_3{\cdot}9H_2O$ dissolved in 122 mL of deionized water (Mg/Al = 2.5/1) was mixed in a colloid mill rotating at 3000 rpm with a solution of 0.40 mol of NaOH and 0.14 mol of Na_2CO_3 dissolved in 122 mL of deionized water. In 2 min, the resulting slurry was transferred to an autoclave for static crystallization at 100 °C for 8 h. The concentration of the alkali solution was related to metal ion concentration in $[NaOH] = 1.6\,[Mg^{2+} + Al^{3+}]$ and $[CO_3^{2-}] = 2.0\,[Al^{3+}]$. The final precipitate was filtered, washed thoroughly with deionized water to pH = 7, and dried at 100 °C for 12 h. The actual Mg/Al ratio in the final product was determined by ICP technique as 2.55. Thus, the resulting solid was denoted $Mg_{2.55}Al{-}CO_3^{2-}$ LDH.

L-tartaric acid (0.008 mol) and $Mg_{2.55}Al{-}CO_3^{2-}$ LDH were mixed in 50 mL of deionized water or *n*-butanol. The dosage of L-tartaric acid was twice as many as the Al (III) moles in $Mg_{2.55}Al{-}CO_3^{2-}$ LDH. The resulting suspension was refluxed for 10 h. The solid was centrifuged, washed with anhydrous ethanol (3 × 50 mL), dried under vacuum at 80 °C overnight, and designated as TA-LDHs (wherein TA represents the tartrate anions).

A mixture of titanium tetraisopropoxide (10 mmol) and TA-LDHs in anhydrous CH_2Cl_2 (30 mL) was stirred for 2 h at room temperature. The input amount of TA-LDHs was determined to ensure a molar ratio of 5 of Ti (IV) to interlayer tartrate. The resulting solid was washed with anhydrous CH_2Cl_2 (50 mL) and anhydrous ethanol (3 × 30 mL), dried overnight under vacuum at 25 °C, and designated as TAT-LDHs.

2.3. Characterization

X-ray diffraction patterns were taken on a Shimadzu XRD-6000 diffractometer with Cu K_α radiation (40 kV and 30 mA) at a scanning rate of 5°/min. FT-IR spectra were recorded on a Bruker Vector 22 spectrometer with a resolution of 4 cm^{-1} using the standard KBr pellet method. The content of Mg, Al, and Ti was determined using ICP emission spectroscopy on a Shimadzu ICPS-7500 ICP instrument by dissolving the samples in dilute HNO_3. ^{13}C CP/MAS NMR spectra were recorded on a Bruker AV300 NMR spectrometer at resonance frequency of 75.47 MHz. The chemical shifts were given relative to TMS as the external reference. SEM and energy dispersive X-ray (EDX) images were taken on a Zeiss Supra 55 scanning electron microscope equipped with an EDX spectroscope. The accelerating voltage applied was 20 kV.

2.4. Catalytic sulfoxidation

Typically, in a sealed 50-mL Erlenmeyer flask, MPS (1.0 mmol), catalyst (equivalent to 0.050 mmol of Ti (IV)), and solvent (10 mL) were first bubbled with nitrogen gas, and then stirred for 1 h at room temperature and another 1 h at 273 K. The reaction was started by the addition of 30% aqueous H_2O_2 as oxidant. The oxidant (in 10 mol% excess of MPS) was added slowly using a microliter syringe under vigorous stirring, with 10 s interruption between each drop. The reaction mixture was sampled at intervals. The sample was added with 0.03 g of Na_2SO_3 to terminate the reaction, and then filtered using a 0.20 μm microfilter. The filtrate was analyzed for ee determination by HPLC (Shimadzu LC-10AD; Daicel chiral OB-H; *n*-hexane/*i*-proponal = 80/20; flow rate: 0.5 ml/min; UV/vis spectrometer: 254 nm). Conversion and selectivity were detected on Shimadzu 2010 GC–MS instrument with a silicone capillary column (DB-5, poly (5% diphenyl-95% dimethylsiloxane, 25 m × 0.2 mm, 0.33 μm film thickness).

3. Results and discussion

3.1. Interlayer arrangement of tartrate anions

Fig. 1 illustrates the powder XRD patterns of the LDHs intercalated with tartrate in deionized water and *n*-butanol as the solvents, as well as that of the $Mg_{2.55}Al{-}CO_3$ LDH as intercalated precursor. As shown in Fig. 1a, the $Mg_{2.55}Al{-}CO_3$ LDH as precursor, displaying the XRD patterns characteristic of hydrotalcite-like materials [25], gives a basal spacing of 0.77 nm calculated from the (003) diffraction at $2\theta = 11.6°$, and an interlayer spacing of 0.29 nm by subtract-

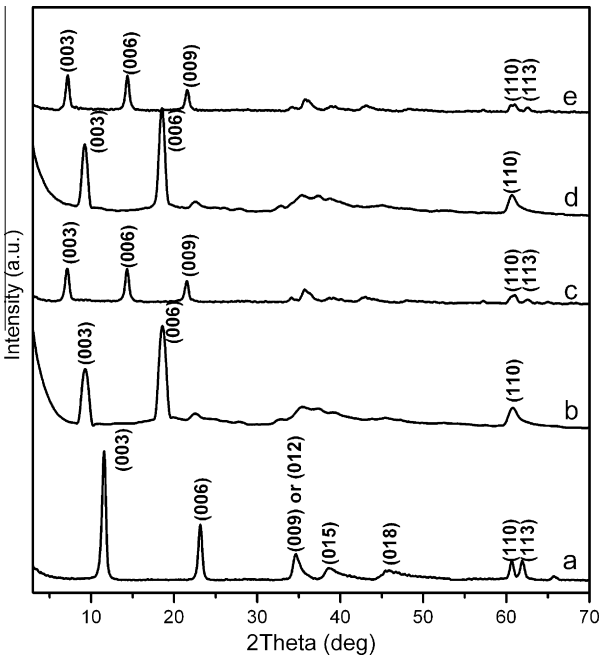

Fig. 1. XRD patterns of (a) $Mg_{2.55}Al{-}CO_3^{2-}$ LDH, after intercalation of (a) with tartrate in (b) *n*-butanol and (c) deionized water, and (d) after coordination of (b) with $Ti(O^iPr)_4$ and (e) coordination of (c) with $Ti(O^iPr)_4$.

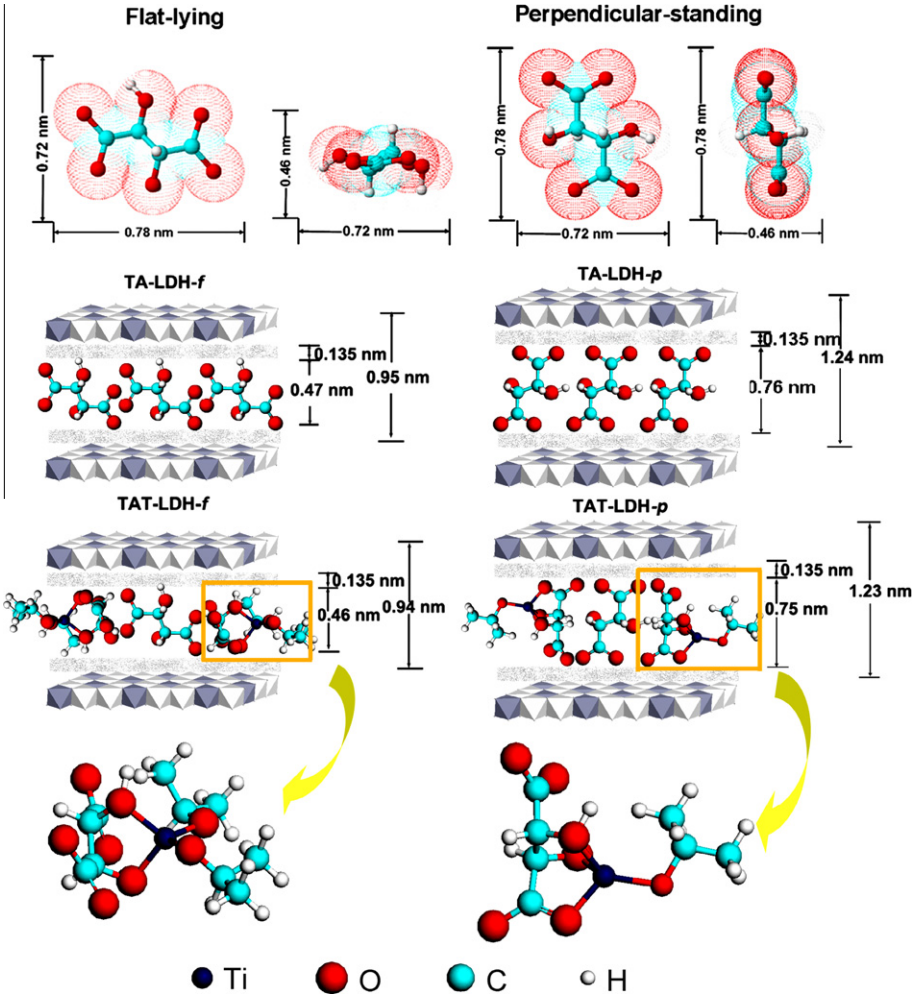

Fig. 2. The dimension of tartrate anion (top), the proposed arrangement of interlayer tartrate (middle), and coordination of interlayer tartrate with Ti (IV) center (bottom).

ing the thickness of the brucite-like layers (0.48 nm) from the basal spacing. For the LDH intercalated with tartrate in *n*-butanol (Fig. 1b), the (003) reflection appears around 9.3°. The basal spacing is calculated to be 0.95 nm, affording an interlayer spacing of 0.47 nm. For the LDH intercalated with tartrate in deionized water (Fig. 1c), the (0 0 3) reflection appears around 7.2°. The basal spacing is calculated to be 1.24 nm, giving an interlayer spacing of 0.76 nm. According to ICP analysis results, the tartrate intercalation in *n*-butanol caused the Mg/Al ratio to increase from 2.55 to 2.62, while decrease to 2.11 in water. This can be explained with the difference in the interference of brucite-like layers by the tartaric acids in *n*-butanol and water. In addition to exchanging the interlayer carbonate, the tartaric acid may disturb the brucite-like layers. The pK_a value of $Mg(OH)_2$ was reported as 11.5 [26], and the pK_a value of $Al(OH)_3$ was reported as 9.36 [27]. Thus, in water, tartaric acid serves as an acidic reagent to dissolve $Mg(OH)_2$ preferentially to $Al(OH)_3$ from the brucite-like layer. But in *n*-butanol, the tartaric acid mainly serves as a coordinating reagent to dissolve Al (III) preferentially from the brucite-like layer because Al (III) has a stronger tendency than Mg (II) toward displacement of protons from the hydroxyl groups of hydroxy acids [28]. The decreased Mg/Al ratio provides larger charge density in the brucite-like layers, allowing the interlayer tartrate anions to be orientated in a denser arrangement. The increased Mg/Al ratio allows the interlayer tartrate anions to be arranged in expanding modes.

The dimension of tartrate anion was measured to be 0.78 × 0.72 × 0.46 nm (including the van der Waals radii for the oxygen and hydrogen atoms) using material studio program, which is illustrated in Fig. 2. One tartaric acid holds two carboxylic groups. The successive pK_a values of tartaric acid are 3.04 and 4.37, both higher than the pK_a values of carbonic acid (6.38 and 10.25). Thus, both carboxylic groups in one tartaric acid are to be deprotonated in the intercalation, substituting the carbonates as interlayer anions. Depending on the orientation of interlayer tartrate, the interlayer spacing of tartrate-intercalated LDH is supposed to be in the range of 0.46–0.78 nm when the interlayer tartrate is in a monolayer arrangement, consistent with the XRD observations. For the LDH intercalated with tartrate in *n*-butanol, the observed interlayer spacing coincides well with the smallest dimension of the tartrate anion. The interlayer tartrates should take an orientation with their largest dimension parallel to the brucite-like layer (“flat-lying”). The resulting intercalate is hereafter abbreviated as TA-LDH-*f*. For the LDH intercalated with tartrate in water, the observed interlayer spacing accords with the largest dimension of the tartrate anion, indicating that the interlayer tartrate takes a “perpendicular-standing” arrangement. The resulting intercalate is hereafter abbreviated as TA-LDH-*p*. The observed interlayer spacing is only shorter by 0.02 nm than the largest dimension of tartrate anion, suggesting a negligible tilt of the anions. The schematic structures of the LDHs with the interlayer tartrate arranged in flat-lying and perpendicular-standing orientations are shown in Fig. 2.

Table 1 lists the area per charge ($A_{c,\ layer}$) and charge density ($D_{c,\ layer}$) of the brucite-like layer of tartrate-intercalated LDHs, calculated from lattice parameter *a* and Mg/Al molar ratio. To balance

Table 1
Structural parameters of intercalated products.

	$Mg_{2.55}Al—CO_3^{2-}$ LDH	TA-LDH-*p*	TAT-LDH-*p*	TA-LDH-*f*	TAT-LDH-*f*
Interlayer spacing (nm)	0.29	0.76	0.75	0.47	0.46
a (nm)	0.306	0.304	0.304	0.304	0.304
Mg/Al molar ratio	2.55	2.11	2.10	2.62	2.62
$A_{c,\ layer}$[a] (nm^2)	0.29	0.25	0.25	0.29	0.29
$D_{c,\ layer}$[a] (e/nm^2)	3.47	4.00	4.00	3.50	3.50
2D-density (number of anion/nm^2)	1.73	2.00	2.00	1.75	1.75

[a] $A_{c,\ layer}$ represents the area unit charge of the brucite-like layer. $A_{c,\ layer} = a^2\sin60°/x$, *x* equals to the molar ratio of Mg/(Mg + Al). $D_{c,\ layer}$ represents the charge density of the brucite-like layer. $D_{c,\ layer} = 1/A_{c,\ layer}$.

the charge of brucite-like layer of TA-LDH-*p*, the area per charge of the interlayer tartrate ($A_{c,\ tartrate}$) should be not larger than 0.25 nm^2. To balance the charge of brucite-like layer of TA-LDH-*f*, $A_{c,\ tartrate}$ should be not larger than 0.29 nm^2. According to the dimensions of tartrate anion, $A_{c,\ tartrate}$ compensated by one perpendicular-standing tartrate anion is 0.17 nm^2 for the monolayer arrangement, and 0.28 nm^2 by one flat-lying tartrate anion for the monolayer arrangement. Either of the $A_{c,\ tartrate}$ value satisfies the requirement of charge compensation. The number of the perpendicular-standing tartrate anions arranged under per square nanometers of LDH slabs is estimated as 2 for TA-LDH-*p*. For TA-LDH-*f*, 1.75 flat-lying tartarte anions are accommodated under per square nanometers. The 2D-densities of the interlayer tartrate are comparable in TA-LDH-*f* and TA-LDH-*p*.

Fig. 3 shows the FT-IR spectra of tartrate-intercalated LDHs and sodium tartrate. For sodium tartrate (Fig. 3a), the asymmetric and symmetric vibrations of —COO— appear at 1622 and 1411 cm^{-1}. The $\Delta\upsilon$ ($\Delta\upsilon = \upsilon_{as} - \upsilon_s$) is calculated to be 211 cm^{-1}, indicative of the bridge symmetry of —COO— groups, consistent with that recognized previously [29]. The band assigned to the —C—O vibration of the alcoholic group appears at 1112 cm^{-1}, and the one assigned to the —CO—H vibration appears at 1067 cm^{-1}. For TA-LDH-*f* (Fig. 3b), the asymmetric vibration of —COO— exhibits overlapped bands centered at 1654 cm^{-1} with a resolved band at 1664 cm^{-1} and another shoulder band at 1608 cm^{-1}, and the symmetric vibration of —COO— centered at 1398 cm^{-1}. The splitting of the asymmetric vibration suggests the diversity in the symmetry of the interlayer carboxylate groups due to its interaction with the brucite-like layers. Two calculated $\Delta\upsilon$ values ($\Delta\upsilon_1 = 266\ cm^{-1}$ and $\Delta\upsilon_2 = 210\ cm^{-1}$) suggest the co-existence of monodentate and bidentate interactions of tartrate carboxylate with the brucite-like layer. That is, the interactions with the brucite-like layers result in the diversified symmetry and the un-equivalence of the carboxylate groups in the flat-lying interlayer tartrate anions. For TA-LDH-*p* (Fig. 3d), the asymmetric vibration of —COO— exhibits one strong band at 1618 cm^{-1}, and the symmetric vibration of —COO— appears at 1398 cm^{-1}. The $\Delta\upsilon$ is 220 cm^{-1}, close to that of the sodium salt, suggesting the approximately bidentate interaction of tartrate carboxylate with the brucite-like layer. Single $\Delta\upsilon$ suggests that the carboxylate groups in perpendicular-standing tartrate approach identical in symmetry. In both TA-LDH-*f* and TA-LDH-*p*, the absence of the band around 1740 cm^{-1}, attributed to the carboxylic group of L-tartaric acid [23], implies the total deprotonation of the L-tartaric acid in the intercalation. The intercalation into LDH interlayer regions causes the splitting of alcoholic vibrations, as can be recognized from Fig. 3. For TA-LDH-*f* (Fig. 3b), the —C—O vibration splits into 1158 and 1095 cm^{-1}, and the —CO—H vibration splits into 1130 and 1061 cm^{-1}. For TA-LDH-*p* (Fig. 3d), the —C—O vibration splits into 1161 and 1092 cm^{-1}, and the —CO—H vibration splits into 1123 and 1046 cm^{-1}. The splitting of alcoholic absorption is attributed to the multiple interactions in the confined interlayer regions, which can be further deduced from the ^{13}C CP/MAS NMR spectra shown in Fig. 4. For pristine L-tartaric acid (Fig. 4a), the chemical shift representing the carboxylic carbon is

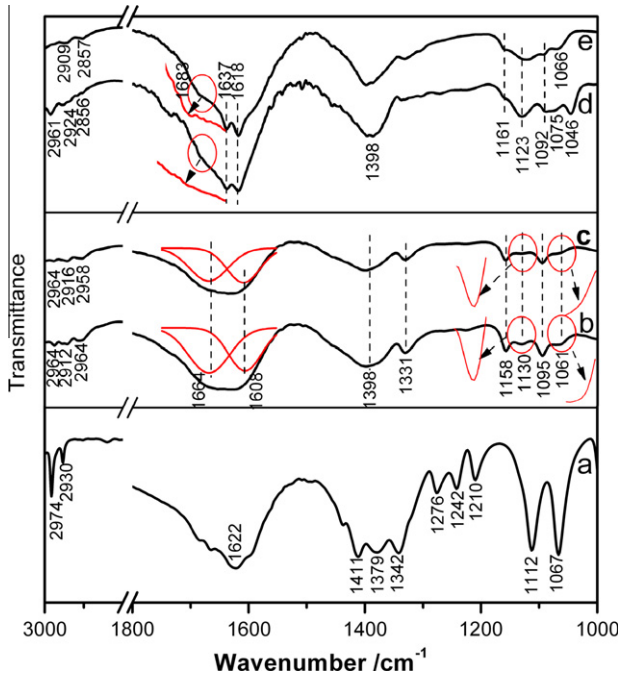

Fig. 3. FT-IR spectra of (a) sodium tartrate; (b) TA-LDH-*f*, (c) TAT-LDH-*f*; (d) TA-LDH-*p*, and (e) TAT-LDH-*p*. The red lines are the amplifications of the circled regions. (For interpretation of the references to colour in this figure legend, the reader is referred to the web version of this article.)

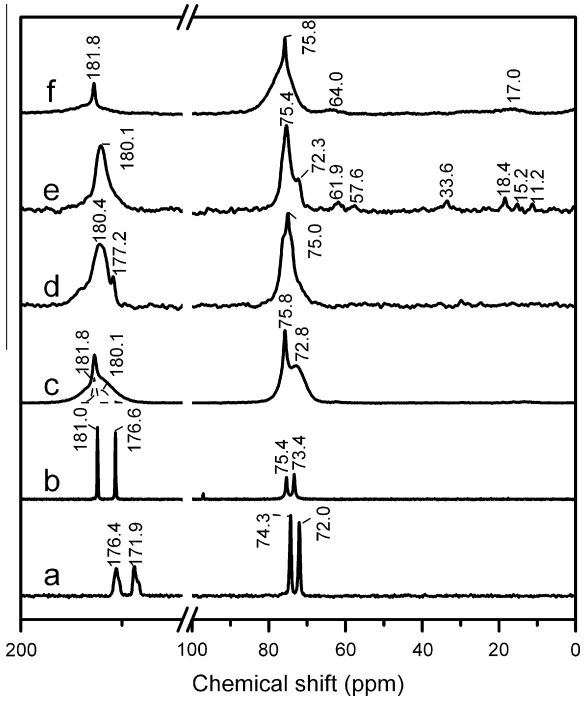

Fig. 4. ^{13}C CP/MAS NMR spectra of (a) L-tartaric acid, (b) sodium tartrate, (c) TA-LDH-*f*, (d) TA-LDH-*p*, (e) TAT-LDH-*f* and (f) TAT-LDH-*p*.

observed at 176.4 and 171.9 ppm, while the alcoholic carbon at 72.0 and 74.3 ppm. For the sodium tartrate salt (Fig. 4b), the chemical shift representing the carboxylate carbon is observed at 180.0 and 176.6 ppm, while the alcoholic carbon at 73.4 and 75.4 ppm. For TA-LDH-*f* (Fig. 4c), the deprotonated carboxylate carbon of the interlayer tartarte exhibits a broad signal enveloping 181.8 and 180.1 ppm. The signals of alcoholic carbon shift downfield to 75.8 ppm with a shoulder at 72.8 ppm. When the tartrate anions are confined in the LDH interlayer space in flat-lying orientation, the alcoholic carbons and carboxylate carbons both approach homogeneity in chemical environment. For TA-LDH-*p* (Fig. 4d), the alcoholic carbon signals merge, exhibiting a broad signal at 75.0 ppm. The deprotonated carboxylate carbons shift upfield to 180.4 ppm with a shoulder downfield at 177.2 ppm, resembling sodium tartrate with bridge symmetry of —COO— groups. When the tartrate anions are confined in the LDH interlayer space in perpendicular-standing orientation, the alcoholic carbon reaches while carboxylated carbon approaches homogeneity in chemical environment. The above observations are reasonable because the brucite-like layers compel the oriented interlayer tartrate anions to rotate in a constrained mode. The flat-lying tartrates suffer more severe restriction than the perpendicular-standing tartrate. In either TA-LDH-*f* or TA-LDH-*p*, no signal around 170 ppm characteristic of carbonate anions is resolved, indicating the LDH interlayer region is occupied completely with tartrate anions.

3.2. In situ coordination to Ti (IV) centers

The coordination of Ti (IV) centers to the intercalated tartrate ligands was carried out by in situ incorporating $Ti(O^iPr)_4$ with TA-LDH-*f* or TA-LDH-*p* in anhydrous dichloromethane. In the XRD patterns of either coordinated product, TAT-LDH-*f* (Fig. 1d) or TAT-LDH-*p* (Fig. 1e), the (0 0 *l*) reflections are observed at the same 2θ as that observed before Ti (IV) coordination, indicating that the in situ coordination to Ti (IV) made no visible effects on the interlayer spacing. As can be seen from the EDX analysis (Fig. 5), more Ti (IV) has been incorporated at the edges than the center regions of platelet-like LDH particles for both TAT-LDH-*p* and TAT-LDH-*f*. It is apparent that some interlayer tartartes, especially those at the center regions, remain uncoordinated to Ti (IV) centers. Although the EDX results have not been fitted with ZAF correction, it could be observed that the Ti (IV) population in TAT-LDH-*p* is larger than that in TAT-LDH-*f* at either edges or central regions. The higher Ti content in TAT-LDH-*p* than in TAT-LDH-*f* is confirmed by ICP elemental analysis. The Ti content has been determined by ICP technique as 0.73% for TAT-LDH-*p*, while 0.32% for TAT-LDH-*f*.

For TAT-LDH-*p*, a band at 1683 cm^{-1} is observed in the FT-IR spectrum (Fig. 3e), which is absent for TA-LDH-*p* (Fig. 3d), suggesting the coordination of C=O with Ti (IV), consistent with that reported previously [30,31]. The weakness in intensity is due to the insufficiency of the C=O—Ti coordination mode. The coordination mode is also supported by the shift of the carboxylate resonance downfield to 181.8 ppm (Fig. 4f). Meanwhile, the constrained rotation of interlayer tartrate results in the homogeneity of carboxylate carbons. The —CO—H vibration at 1046 cm^{-1} vanishes and the one at 1123 cm^{-1} fades, and meanwhile a new band at 1066 cm^{-1} emerges (Fig. 3e), suggesting the coordination of tartrate alcoholic moieties to Ti (IV) centers. The alcoholic carbon resonance shifts downfield to 75.8 ppm (Fig. 4f) due to the formation of —C—O—Ti (IV) coordination, consistent with that observed previously [32]. The —O^iPr resonances at 64.0 and 17.0 ppm are quite obscure, consistent with the substitution of —O^iPr by tartrate as ligands. A majority of —O^iPr moieties has been eliminated from Ti (IV) centers in TAT-LDH-*p*.

For TAT-LDH-*f*, the vibrations of —CO—H at 1130 and 1061 cm^{-1} fade in the FT-IR spectrum (Fig. 3c), suggesting the coordination of tartrate alcoholic moieties to Ti (IV) centers. But no CO—Ti absorption is resolved due to the low Ti (IV) population in TAT-LDH-*f*. In the ^{13}C CP/MAS NMR spectrum (Fig. 4e), the resonance of alcoholic carbons hardly shift, because the low Ti (IV) population allows most interlayer tartrate to remain in coordination-free mode. The asymmetric and symmetric vibrations of carboxylate group appear at 1664, 1608, and 1398 cm^{-1} in the FT-IR spectrum (Fig. 3c), no obvious shift observed after Ti (IV) coordination. The carboxylate moieties in flat-lying tartrates are supposed to suffer steric restriction from the brucite-like layers, and thus be inhibited from coordinating to Ti (IV). Accordingly, the signals associated with —O^iPr moieties at 61.9, 33.6 and 18.4 ppm are clearly observed. More —O^iPr moieties have been preserved in TAT-LDH-*f* than TAT-LDH-*p*.

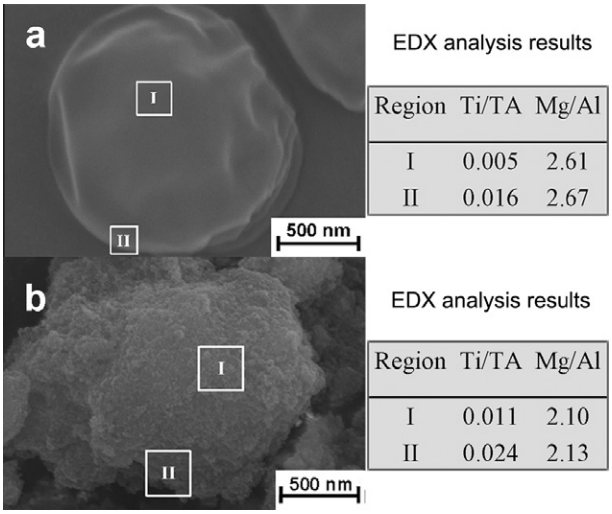

Fig. 5. EDX analyses of (a) TAT-LDH-*f* and (b) TAT-LDH-*p*. The selected square regions (I and II) were characterized by EDX. The absorption intensity of the elements in the selected regions has not been fitted atomic number (*Z*)-absorption-fluorescence (ZAF) correction.

The proposed coordination modes according to the above discussions are schematically illustrated in Fig. 2. The perpendicular-standing interlayer tartrate facilitates its coordination to Ti (IV) centers, while the interlayer tartrate anion in flat-lying orientation suffers more restriction from the interlayer space. In TAT-LDH-*f*, Ti (IV) centers are coordinated with interlayer tartrate in bidentate mode through C—O—Ti linkages. In TAT-LDH-*p*, Ti (IV) centers are coordinated with interlayer tartrate in multidentate modes by both C=O—Ti and C—O—Ti linkages.

Fig. 6a shows the in situ temperature-programmed XRD patterns of TAT-LDH-*p*. The (0 0 3) reflection gradually shifts from 7.2° to 8.9° with the temperature increasing from 298 to 473 K. The basal spacing changes from 1.23 to 0.99 nm, reduced in 0.24 nm. This observed contraction of basal spacing, similar to the thickness of bilayer hydrogen-bonding region, is associated with the removal of the interlayer water molecules. Similar contraction of basal spacing is observed for TA-LDH-*p* (Fig. 6b). Further heating TAT-LDH-*p* causes the (0 0 *l*) reflections to fade away. The layered structure collapses at 623 K, as indicated by the absence of (0 0 *l*) reflections. Meanwhile, the reflections characteristic of cubic MgO-like phase appear, resulting from the de-hydroxylation of the brucite-like layers. Anatase TiO_2 phase emerges at 723 K, due to the decomposition and subsequently aggregation of Ti (IV) species.

3.3. Asymmetric catalysis in sulfoxidation

The TAT-LDHs have been applied as catalysts for the heterogeneous sulfoxidation of MPS in organic solvents at 273 K, yielding the corresponding MPSO as the absolutely major product. The re-

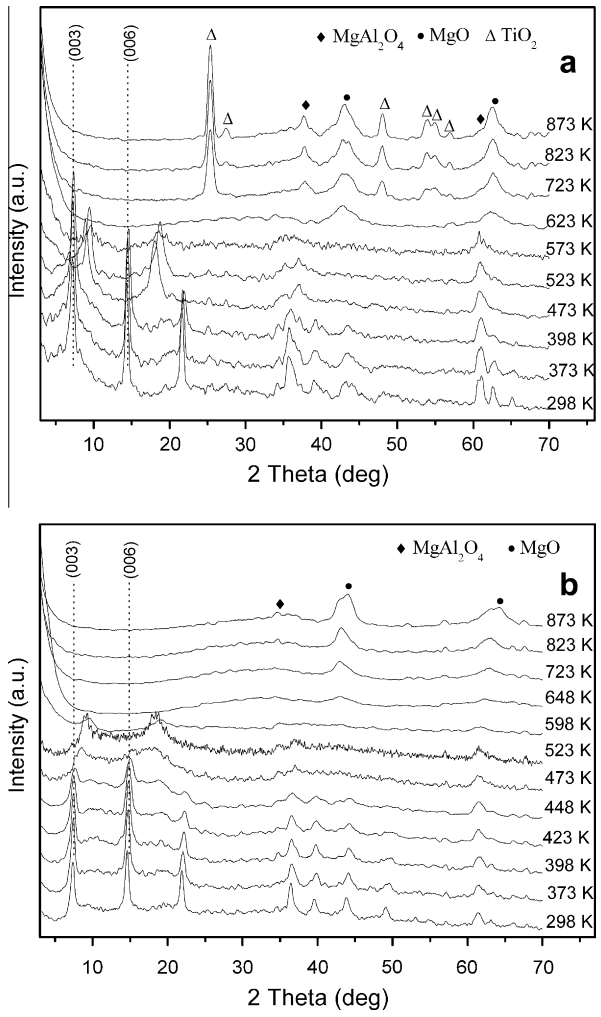

Fig. 6. In situ temperature-programmed XRD patterns of (a) TAT-LDH-*p* and (b) TA-LDH-*p*.

sults are shown in Table 2. In the control reactions (Entries 1–3), which was carried out in the presence of $Mg_{2.55}Al{-}CO_3^{2-}$ LDHs while without Ti (IV) introduced, a sulfide conversion of less than 3% is observed in 9 h. No visible oxidation in CH_3CN as solvent (Entry 1) has been detected, indicating the Payne-Reagent [33] combining H_2O_2 and CH_3CN is invalid in our system. The oxidation reactions in weak polar solvent CH_2Cl_2 hardly occur, giving neglectable MPS conversion and ee (Entries 4 and 5). In the protic solvent MeOH (Entries 6 and 7), the MPS conversion has been markedly improved. However, the ee value is poor. Decreasing the polarity of solvent by mixing MeOH with CH_2Cl_2 in MeOH/CH_2Cl_2 = 1/1 (Entries 8 and 9), no obvious improvement of ee has been achieved. Using CH_3CN as solvent (Entries 10 and 11), which is less polar than MeOH, more polar than MeOH/ CH_2Cl_2 mixture, and much more polar than CH_2Cl_2, the ee has been greatly enhanced, while the MPS conversion is observed to decrease. The results suggest that, in the asymmetric sulfoxidation catalyzed by the Ti (IV) centers coordinated to pre-intercalated tartrate, the MPS conversion is favored by highly polar or preferably protic solvent, while the enantioselectivity prefers a solvent with medium polarity. As the control, the homogeneous counterpart, pre-formed Kagan's titanium-tartrate complex [23], exhibits poor enantioselectivities in all the selected solvents (Entries 14–16).

The enhancement of MPS conversion by protic solvent was also previously observed in the sulfoxidation using Ti-containing zeolites as catalysts [34]. The protic solvent was supposed to coordinate to the active peroxo-Ti (IV) species, thereby decreasing the electron density of the activated Ti (IV) sites [35]. In our system, the polar solvent additionally facilitates the solvated reactants to diffuse into the hydrophilic interlayer regions of TAT-LDH-*p* and TAT-LDH-*f*, increasing their access to the interlayer catalytic sites. The significance of matching solvent polarity to the hydrophilicity/hydrophobicity of interlayer regions has actually been revealed in our previous study [24]. On the LDHs intercalated with preformed Kagan's titanium-tartrate complex (Mg/Al–Ti (IV) TA_2) [23], in which the Ti (IV) TA_2 complexes were arranged in an interdigitated bilayer with their hydrophobic alkoxyl groups interlacing in the interlayer regions of LDHs, a minor conversion of MPS was observed in CH_3CN [24]. It resulted from the difficulty for CH_3CN in diffusing into the hydrophobic interlayer regions of Mg/Al–Ti (IV) TA_2. But it is much easier for CH_3CN to diffuse into the hydrophilic interlayer space of TAT-LDH-*p* or TAT-LDH-*f*, giving a significant MPS conversion. The catalytic reaction occurring in the interlayer regions was found to produce higher enantioselectivity due to the confinement of the LDH interlayer space [24], which also accounts for the higher ee observed in CH_3CN for TAT-LDH-*p* and TAT-LDH-*f*. But the participation of achiral protic solvent disfavors the asymmetric induction even when the catalytic reactions occur inside the confined interlayer regions. Different from the activated Ti (IV) centers in Mg/Al–Ti (IV) TA_2, which were saturated in hexacoordinates with tartrate and peroxo [24], the activated Ti (IV) centers in TAT-LDH-*p* or TAT-LDH-*f* are penta- or tetra-coordinated.

Table 2
Catalytic sulfoxidation on TAT-LDH-*f* and TAT-LDH-*p*.

Entry	Catalyst	Solvent	Oxidant	Time (h)	Conv. (%)	Selectivity of MPSO (%)	ee (%)
1	$Mg_{2.55}Al{-}CO_3^{2-}$ LDH	CH_3CN	H_2O_2	9	2	100	nd[a]
2	$Mg_{2.55}Al{-}CO_3^{2-}$ LDH	MeOH/CH_2Cl_2	H_2O_2	9	1	100	nd
3	$Mg_{2.55}Al{-}CO_3^{2-}$ LDH	MeOH	H_2O_2	9	3	100	nd
4	TAT-LDH-*p*	CH_2Cl_2	H_2O_2	9	1	100	2
5	TAT-LDH-*f*	CH_2Cl_2	H_2O_2	9	2	100	3
6	TAT-LDH-*p*	MeOH	H_2O_2	9	95	98	14
7	TAT-LDH-*f*	MeOH	H_2O_2	9	87	96	2
8	TAT-LDH-*p*	MeOH/CH_2Cl_2	H_2O_2	9	57	100	21
9	TAT-LDH-*f*	MeOH/CH_2Cl_2	H_2O_2	9	48	100	2
10	TAT-LDH-*p*	CH_3CN	H_2O_2	9	33	84	58
11	TAT-LDH-*f*	CH_3CN	H_2O_2	9	20	96	41
12	TAT-LDH-*p*	CH_3CN	TBHP	9	5	100	57
13	TAT-LDH-*f*	CH_3CN	TBHP	9	6	100	36
14	Ti(IV)-tartrate	CH_3CN	H_2O_2	1	42	93	2
15	Ti(IV)-tartrate	MeOH/CH_2Cl_2	H_2O_2	3	50	87	2
16	Ti(IV)-tartrate	MeOH	H_2O_2	2	90	97	4

[a] nd is short for not determined.

There are coordinative vacancies available for protic solvent in TAT-LDH-*p* and TAT-LDH-*f*, thus giving inferior enantioselectivity. The Ti leaching is monitored not more than 16% for TAT-LDH-*f* and 14% for TAT-LDH-*p* in MeOH. In CH_3CN, the Ti leaching is negligible for TAT-LDH-*f* and not more than 7% for TAT-LDH-*p*. In light of the above results, it is worthy of note that the appropriate match between the polarity of reaction solvent and the hydrophobicity/hydrophilicity of catalytic regions is significantly critical for the asymmetric catalysis, at least for the catalyst with its catalytic sites intercalated in the bi-dimensional interlayer space.

The results in Table 2 also show that, in each case, the TAT-LDH-*p* as catalyst produces higher activity and better enantioselectivity than TAT-LDH-*f*. The higher activity of TAT-LDH-*p* is supposed to result from its larger interlayer spacing, which facilitates the access of both oxidants and MPS to the interlayer Ti (IV) centers. The better asymmetric induction of TAT-LDH-*p* is supposed to result from the Ti (IV)-tartrate coordination modes. As discussed above, the Ti (IV) centers in TAT-LDH-*f* hold only C—O—Ti coordination, while the ones in TAT-LDH-*p* hold C=O—Ti coordination besides C—O—Ti. That is, in TAT-LDH-*p*, the coordination structure suffers [2.2.1] bicylic strain, constructing a more rigid chiral backbone, which was reported to be the origin of enantioselectivity [36]. As schematically illustrated in Fig. 7, although the peroxo-Ti (IV) species formed by the η-coordination of hydrogen peroxide are similar for both TAT-LDH-*f* and TAT-LDH-*p*, a discrepancy comes forth in the subsequent attack of MPS because of the bicylic strain in TAT-LDH-*p*. The Si-face attack is inhibited using TAT-LDH-*p* as catalyst, producing an excess of (R)-configured MPSO. Using TAT-LDH-*f* as catalyst, the attack of MPS to the activated Ti (IV) centers in either Re-face or Si-face direction is unprivileged, as a result of the less stereo strain from the tartrate-Ti (IV) coordination.

Using bulky *t*-butyl hydroperoxide (TBHP) as oxidant instead of H_2O_2 (Entries 12 and 13), the MPS conversion decreases in comparison with the H_2O_2 system, because it is difficult for the bulky oxidant to access the interlayer Ti (IV) centers. But the chiral induction of either TAT-LDH-*p* or TAT-LDH-*f* has been preserved, benefiting from the spatial restriction of bulky *t*-butyl moiety in the attack of MPS to the active peroxo-Ti (IV) species.

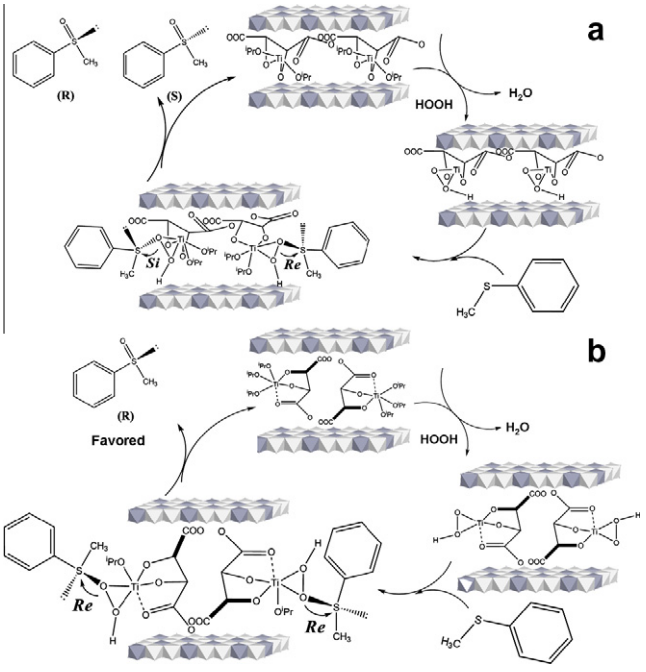

Fig. 7. Proposed catalytic mechanism of (a) TAT-LDH-*f* and (b) TAT-LDH-*p*.

It has been demonstrated in this work that pre-intercalation of tartrate ligands to coordinate to Ti (IV) sites is a promising approach in that it produces enantioselectivity while the homogeneous counterpart gives racemic products in the asymmetric sulfoxidation. Moreover, it provides a possibility of further enhancing enantioselectivity by controlling the coordination modes in virtue of tunable orientation of ligand anions in the interlayer regions of layered host. The question encountered for the moment is how to increase the Ti (IV) loading. The insufficient loading here is supposed to result from the poor affinity between the hydrophilic LDH interlayer regions and the apolar medium (CH_2Cl_2) in the in situ coordination. Our recent work demonstrates that the Ti (IV) population can be elevated by using polar solvents as the coordination medium. The Ti (IV) content has been increased to 1.47% in acetonitrile, 10.41% in dimethylformamide, and 12.70% in *n*-butanol for TAT-LDH-*p*.

4. Conclusions

In conclusion, the Ti (IV) complex as the catalytic site for asymmetric sulfoxidation has been immobilized in the interlayer region of layered double hydroxide by pre-intercalation of chiral tartrate as ligand to coordinate to Ti (IV). It has been found that the orientation of interlayer tartrate makes impact on their coordination modes to Ti (IV) centers, and then on the catalytic activity and asymmetric induction. The catalytic sites with the tartrate ligand in perpendicular-standing orientation and the Ti (IV) center coordinated in both C—O—Ti and C=O—Ti modes display higher catalytic activity and better chiral induction in the asymmetric sulfoxidation.

Acknowledgment

The authors are grateful to the financial support from NSFC and "973" Program (2011CBA00504).

Reference

[1] M. Heitbaum, F. Glorius, I. Escher, Angew. Chem. Int. Ed. 45 (2006) 4732.
[2] Q.H. Fan, C.Y. Ren, C.H. Yeung, W.H. Hu, A.S.C. Chan, J. Am. Chem. Soc. 121 (1999) 7407.
[3] Y. Uozumi, H. Tanaka, K. Shibatomi, Org. Lett. 6 (2004) 281.
[4] M.J. Farrall, M. Alexis, M. Trecarten, Nouv. J. Chim. 7 (1983) 449.
[5] L. Canali, J.K. Karjalainen, D.C. Sherringtona, O. Hormi, Chem. Commun. (1997) 123.
[6] S. Xiang, Y.-L. Zhang, Q. Xin, C. Li, Angew. Chem. Int. Ed. 41 (2002) 821.
[7] A. Cornejo, J.M. Fraile, J.I. García, E. García-Verdugo, M.J. Gil, G. Legarreta, S.V. Luis, V. Martínez-Merino, J.A. Mayoral, Org. Lett. 4 (2002) 3927.
[8] J.K. Park, S.W. Kim, T. Hyeon, B.M. Kim, Tetrahedron – Asymmetry 12 (2001) 2931.
[9] J.M. Fraile, J.I. García, M.A. Harmer, C.I. Herrerías, J.A. Mayoral, O. Reiserc, H. Werner, J. Mater. Chem. 12 (2002) 3290.
[10] S.A. Raynor, J.M. Thomas, R. Raja, B.F.G. Johnson, R.G. Bell, M.D. Mantle, Chem. Commun. (2000) 1925.
[11] V.J. Mayani, S.H.R. Abdi, R.I. Kureshy, N.H. Khan, A. Das, H.C. Bajaj, J. Org. Chem. 75 (2010) 6191.
[12] J. He, M. Wei, B. Li, Y. Kang, D.G. Evans, X. Duan, Struct. Bond. 119 (2006) 89.
[13] A.I. Khan, D. O'Hare, J. Mater. Chem. 12 (2002) 3191.
[14] S.P. Newman, S.J. Williams, P.V. Coveney, W. Jones, J. Phys. Chem. B 102 (1998) 6710.
[15] T. Itoh, T. Shichi, T. Yui, H. Takahashi, Y. Inui, K. Takagi, J. Phys. Chem. B 109 (2005) 3199.
[16] M. Chibwe, L. Ukrainczyk, S.A. Boyd, T.J. Pinnavaia, J. Mol. Catal. A – Chem. 113 (1996) 249.
[17] Y.F. Chao, P.C. Chen, S.L. Wang, Appl. Clay Sci. 40 (2008) 193.
[18] K.A. Tarasov, D. O'Hare, Inorg. Chem. 42 (2003) 1919.
[19] R. Rojas, M.R. Perez, E.M. Erro, P.I. Ortiz, M.A. Ulibarri, C.E. Giacomelli, J. Colloid Interface Sci. 331 (2009) 425.
[20] N.H. Gutmann, L. Spiccia, T.W. Turney, J. Mater. Chem. 10 (2000) 1219.
[21] M. Wei, X. Zhang, D.G. Evans, X. Duan, X. Li, H. Chen, AIChE J. 53 (2007) 2916.
[22] B.M. Choudary, B. Kavita, N.S. Chowdari, B. Sreedhar, L.M. Kantam, Catal. Lett. 78 (2002) 373.
[23] H. Shi, C. Yu, J. He, J. Phys. Chem. C 114 (2010) 17819.
[24] H. Shi, C. Yu, J. He, J. Catal. 271 (2010) 79.
[25] D.G. Evans, R.C.T. Slade, Struct. Bond. 119 (2006) 1.

[26] G.J. Narlikar, V. Gopalakrishnan, T.S. Mcconnell, N. Usman, D. Herschlag, Proc. Natl. Acad. Sci. 92 (1995) 3668.
[27] J.D. Hem, C.E. Roberson, Geol. Surv. Water-Supply Pap. (US) 1827-A, 1967, p. 55.
[28] R.J. Moterkaitis, A.E. Martell, Inorg. Chem. 23 (1984) 19.
[29] V. Prevot, C. Forano, J.P. Besse, Inorg. Chem. 37 (1998) 4293.
[30] P.G. Potvin, S. Bianchet, J. Org. Chem. 57 (1992) 6629.
[31] M.G. Finn, K.B. Sharpless, J. Am. Chem. Soc. 113 (1991) 113.
[32] M. Kakihana, T. Nagumo, M. Okamoto, H. Kakihana, J. Phys. Chem. 91 (1987) 6128.
[33] W.C. Frank, Tetrahedron – Asymmetry 9 (1998) 3745.
[34] V. Hulea, P. Moreau, J. Mol. Catal. A – Chem. 113 (1996) 499.
[35] G. Bellussi, A. Carati, M.G. Clerici, G. Maddinelli, R. Millini, J. Catal. 133 (1992) 220.
[36] P.G. Potvin, B.G. Fieldhouse, Tetrahedron – Asymmetry 10 (1999) 1661.